Characteristics of CoZrTaB in the 5G Spectral Environment

by

Phillip C. Miller

A Thesis presented in Partial Fulfillment
Of the Requirement for the Degree
Master of Science

Approved April 12 2018 by the
Graduate Supervisory Committee:

Hongbin Yu, Chair
James Aberle
Jennifer Blain Christen

ARIZONA STATE UNIVERSITY

April 2018

ABSTRACT

The study of soft magnetic materials has been growing in popularity in recent years. Driving this interest are new applications for traditional electrical power-management components, such as inductors and transformers, which must be scaled down to the micro and nano scale while the frequencies of operation have been scaling up to the gigahertz range and beyond. The exceptional magnetic properties of the materials make them highly effective in these small-component applications, but the ability of these materials to provide highly-effective shielding has not been so thoroughly considered. Most shielding is done with traditional metals, such as aluminum, because of the relatively low cost of the material and high workability in shaping the material to meet size and dimensional requirements.

This research project focuses on analyzing the variance in shielding effectiveness and electromagnetic field effects of a thin film of Cobalt Zirconium Tantalum Boron (CZTB) in the band of frequencies most likely to require innovative solutions to long-standing problems of noise and interference. The measurements include Near H-Field attenuation and field effects, Far Field shielding, and Backscatter. Minor variances in the thickness and layering of sputter deposition can have significant changes electromagnetic signature of devices which radiate energy through the material.

The material properties presented in this research are H-Field attenuation, H-Field Flux Orientation, Far-Field Approximation, E Field Vector Directivity, H Field Vector Directivity, and Backscatter Magnitude. The results are presented, analyzed and explained using characterization techniques. Future work includes the effect of sputter deposition orientation, application to devices, and applicability in mitigating specific noise signals beyond the 5G band.

Dedicated to

Cathy and the Snuggle-cubs

ACKNOWLEDGEMENTS

Nothing worth having comes without sacrifice.

Mom & Dad, who taught me that Hard Work + Delayed Gratification = Infinite Success

Uncle Jerry, who showed me that you can be a geek and still be cool.

Dr. Dong-ho Han, for setting me on the path.

and

Grandpa, for reminding me that the world needs ditch-diggers, too.

Sincere appreciation to Dr. Hongbin Yu and the members of my committee, for providing the direction and resources needed to explore this subject, share my learning, and grow professionally.

TABLE OF CONTENTS

LIST OF FIGURES

Figure Page

Figure Page

LIST OF TABLES

Table Page

Chapter

1 INTRODUCTION

Motivations

Chromium-Zinc-Boron-Tantalum (CoZrTaB) is a new thin film with distinct magnetic properties. Previous implementations of the material focused on its applicability as a magnetic core in nano-scale inductors. The unique resistivity and magnetic properties documented for the material indicate that it is well-suited to provide effective shielding, and is particularly applicable for Internet-of-Things (IoT) devices and others operating in the 5G spectrum. While much publicity is focused on 5G for cellular phones or other broadband data applications, the initial deployments will be in the Sub-6GHz range for Factory 4.0, Responsive Retail, and the Transportation & Logistics market segments [2]. These devices will have to perform in a wide variety of physical environments with dense populations of similar devices. Because of the low power requirements, advanced signal processing to overcome ambient noise will be problematic, necessitating a shielding method with does not add undo dimensional or thermal consideration. Whenever there is an issue of noise or electromagnetic interference, there are three areas which require consideration: the source of the noise or interference, the coupling mechanism which delivers the noise or interference, and the system or component which is targeted by the noise or interference. Traditional methods of mitigating the harmful of effects of noise have focused on applying a metal shield around the source or the target in order to decouple the harmful energy. However, this comes with several trade-offs, detailed below.

Typical Shielding Implementations.

A typical metal shield as implemented on a printed circuit board (PCB) is a structure which surrounds the device(s) and prevents electromagnetic energy from coupling in to or out of

the physical area under the shield. The shield accomplishes this by providing a directly-coupled path to the reference plane or an inductively reflected path away from the target.

Certain common system components are particularly prone to radiating noise or being particularly susceptible to radiated noise, due to their small size and the presence of high-speed digital or radio-frequency circuits – such as Solid State Drives (SSD) or Radios (Bluetooth, Wi-Fi, LoRA, etc.) with 'module certification'. Module Certification is a regulatory process whereby a Radio is certified in any implementation which is sufficiently similar to the implementation which was tested for certification [3]. One technique commonly used to mitigate the problems with external metal shields on devices which typically radiate noise is to sputter a metal layer on the device. Sputter deposition involves ejecting material from a "target", which is a source onto a "substrate" such as a silicon or polyimide. For example, a solid state drive may have a metal alloy deposited on the top and all 4 vertical sides. This metal is then attached to the reference plane with vias around the Ball-Grid Array (BGA), providing an encapsulating shield. However, a fairly thick shield is required, and it is difficult to provide uniform thickness on horizontal and vertical faces. As the thickness increases, the disparity increases, which may allow current loops to set up on the top of the shield. These current loops can then radiate off shield, compromising the effectiveness of the shield, and even becoming a problem in and of themselves [4].

Thermal.

Because the inductively coupled path for the radiation to return to the reference plane via the shield or other path must be of lower electrical resistance than the path through the source or target, there must be an electrical insulation between the shield and the device. In typical implementations, this is accomplished with an air-gap, although dielectric materials and electrical insulation can be used. The absence of an air-gap or dielectric would provide not only a conductive path for the noise to reach the device, it would also provide a short-circuit path for any signal moving on a surface layer of the PCB. The drawback of this electrically-insulating area is that it is also a thermally-insulating layer. Whenever there is current and resistance, there is

heat. Heat is also detrimental to the proper function of electrical circuits, and must be moved away from the device and the surface of the PCB. This means that the shield must have gaps in order to let air or other coolant move around the device. These gaps in the shield are slot antennas for any noise reverberating under the shield or for any noise that exists in the ambient environment. Shields are designed to minimize the propagation of electromagnetic noise which is known to be harmful through these slot antennas, but a path for certain waves will always be present [5].

Cost.

It is obvious that any time a component is added to a design, the cost of the design increases. Although significant, the cost associated with a traditional metal shield is not limited to the cost of the material plus the cost of installation. Whenever a component which is under a shield fails, it is no longer cost-effective replace that part [6]. In order to do so would require man-hours and materials to remove the shield, identify and replace the part, and then re-install a shield. Shields with removable tops exist, but they are more expensive, less effective, and require skilled labor to remove and install. Generally, these shields are used in prototyping environments where especially expensive or rare parts are under the shield. As a result, most situations in production environments where a defective or non-functioning component is identified under the shield, the entire device is scrapped. In situations where shields are extensively implemented, scrap or rework costs can quickly reach more than $30 million/year. Consider a low-cost IoT device which has a voltage regulation area of the PCB radiating electromagnetic noise, and the solution is to place a shield over the area. In that situation, any single component which fails under the shield would necessitate sending the entire product to scrap, even if that component cost is fractional [7].

Volume.

The presence of a typical metal shield significantly increases the footprint of the device, not just by the dimensions of the shield, but also by the areas of exclusion around the shield

which are required in order to place and attach the shield without harming thermally-sensitive components. While a few millimeters does not initially appear to be a large area, design wins have been achieved by reducing a PCB by less than 4 mm^2 of XY area. Even more costly is the additional height required for a shield. This height includes the thickness of the shield, as well as the air gap under the shield and any heat-dissipating material or space. While electronic devices have dramatically reduced their XY footprint over the previous decades, the reductions in Z-height have been much more difficult to achieve. The primary restriction on Z-height is the metal shields used to minimize noise from intentional radiation sources and/or to minimize the sensitivity of high-speed digital devices.

Reflections/Backscatter.

One of the detriments of shielding that is rarely discussed is the problem of reflecting noise back on to the source. The energy reflected off of the shield doesn't disappear into the ether, it couples on to any suitable conductor in its path, including the traces around the source or on interior layers of the board. This is noise that must be overcome by designing circuits and adding components to maintain signal integrity. Improving digital signal integrity usually involves faster rise and fall times of digital information, and possibly greater amplitude. These actions increase the spectral content of signals, which provides even more sources of noise. Additionally, these devices and circuits require power, and will impact the power delivery requirements.

Objective of Study

The objective of the study is to quantify the effectiveness of the CoZrTaB material when deposited as a thin film using sputter deposition techniques.

The specific objectives are:

- To document the variance of CoZrTaB shielding effectiveness between Polyimide and Silicon substrates

- To evaluate the shielding effectiveness of CoZrTaB on a standing wave of known frequency over a magnetic strapline
- To evaluate the shielding effectiveness of CoZrTaB on modulated signals in the range of frequencies most populated by communication protocols
- To evaluate the shielding effectiveness of CoZrTaB on modulated signals in a band licensed exclusively for 5G devices
- To evaluate the shielding effectiveness of CoZrTaB on a complex wave generated by a nominal device in a worst-case typical usage.

Limitations of Study

The limitations of the study are as follows:

- The time available precludes generating new sputtering samples specifically for the study.
- All samples have been generated as part of unrelated studies, and have been adapted for the purpose of this study.
- One sample, the one constructed of 3 layers of 100nm, has no identifying marks to indicate the orientation of sputter deposition.
- Small sample size decreases statistical power of study, increasing margin of error and possibility of Type II statistical analysis errors. This is a statistical error where the researcher accepts a null hypothesis which is not true. The probability of a test having no Type II errors is referred to as the Power of the test. [1]
- One Device Under Test is a prototype. As such, certain measurement parameters of the reference device are not for publication, but were shared with committee members who had a standing Non-Disclosure Agreement with the manufacturer of the device. While the analysis was ongoing, the test setup had to be returned to the manufacturer. Future availability is certain, but specifics are not known at the time of this writing.

Organization of Thesis

The thesis has been divided in to 5 chapters.

Chapter I Introduction: The primary focus of this chapter is the rationale, limitations, and objectives of the study.

Chapter II Materials and Methodology: The materials used and the methodologies adopted for the study are detailed in this chapter. The parameters of the study and the test methods are briefly reviewed as well.

Chapter III Results and Discussion: The analysis of test results, and accompanying figures, tables, and pictures are presented in this chapter.

Chapter IV Conclusions and Recommendations: The conclusions drawn by the study, and recommendations based on those conclusions, are given in this chapter.

Chapter

2 EXPERIMENTAL TOOLS

Materials

Material samples were repurposed from a previous study, and were not created specifically for the measurements undertaken by this learning. As such, there are limitations in the ability to craft a comprehensive analysis where comparisons are made between a statistically-relevant number of control samples and a similarly sized population of experimental samples, where each experimental sample is altered only by a single source of variance specifically designed for providing information for a data-driven conclusion. Additionally, there was only one sample of a sufficient size and suitable workability to modify for specific measurements. The result of that limitation is that not every sample could be used for every test. Some samples were too small or too large to take congruent measurements, while others were not suitable for certain measurements due to their asymmetric shape. As the number of suitable samples was highly restricted, and there were no redundant or spare samples, there was a risk of damaging samples during measurement and rendering a sample unusable. Special care was taken to minimize the possibility of physical damage or introducing other sources of uncontrolled variance in the single samples, but there was no opportunity to perform repeated measurements due to the risks of damage or changed values due to overuse on a single measurement. This limitation in sample population also restricts the ability of the study to quantify measurement uncertainty, confidence interval, Type II statistical error probability, and margin of error. However, as the purpose of this study is to identify the presence or absence of certain characteristics, and to gauge the relative magnitude of specific types of gross variance in the samples, the results obtained from the study of this population of samples was deemed more than adequate to guide decision-making in future designs of experiments. The population of samples available for experiment are shown in the figure below.

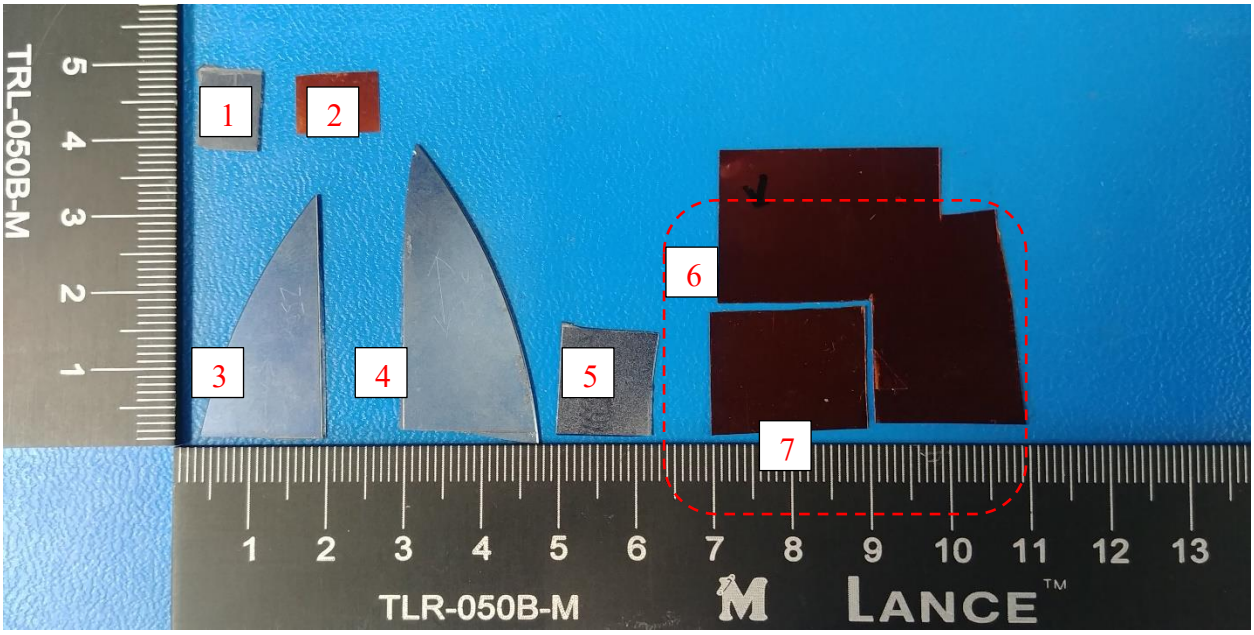

Figure 1. Available samples and their relative sizes

The following table describes the deposition technique, total thickness of CoZrTaB, and substrate material of the samples used in this study.

Table 1. Description of Material Samples

#	Deposition Layers	Layer Thickness (nm)	CoZrTaB Thickness (nm)	Substrate
1	5	5	25	Silicon
2	5	5	25	Polyimide
3	5	100	500	Silicon
4	1	250	250	Silicon
5	3	100	300	Silicon
6	10	50	500	Polyimide
7	10	50	500	Polyimide

Samples are shown with the deposition layer facing down in order to emphasize the difference in substrates. The brownish-red samples have a substrate of 50 micrometer of polyimide, while the blueish-grey samples have a substrate of 500 micrometers of silicon. In this picture, all of the samples are oriented with their respective sputter deposition direction in the vertical axis. The

exception to this is Sample #5, of 3 layers of 100nm, occupying the 5-6cm of the horizontal axis. This is the only sample which did not have an indication scribed on it for the direction of sputter deposition. However, experimentation indicates that the displayed orientation shows the sputter deposition in the same axis as the other samples. The sample to the far right (Sample 6/Sample 7) is the only one which was large enough and of a sufficiently workable material to create a specific sample for measurement. The section shown as having been cut out was taken to provide a full shield for an unshielded SSD. Also of note is that the two smallest samples at the top of the image will have their sputter depositions oriented orthogonally when the samples are oriented congruently.

Devices Under Test

Experimentation was accomplished using three specific devices. Measurements were taken over a reference strip lines designed for 6 GHz, a reference strapline for 20 GHz, and over a prototype Solid State Drive provided by a leading manufacturer. The devices are shown in Figure 2, and detailed information about the specific units can be found in Table 2.

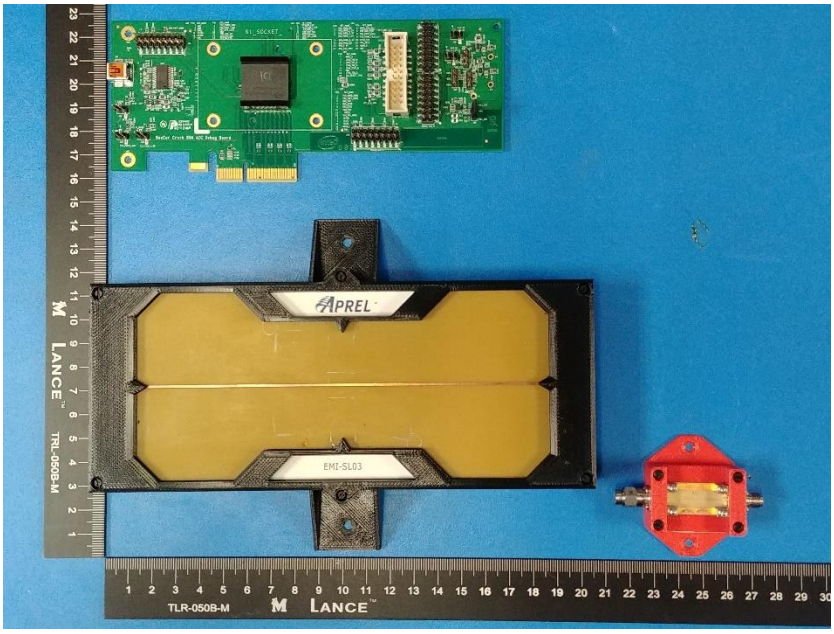

Figure 2. Devices Under Test

Table 2. Description of Devices Under Test

Nomenclature	Manufacturer	Model Number	Serial Number
6 GHz Magnetic Strip line	Aprel		5
20 GHz Magnetic Strip line	Aprel		5
Unshielded SSD	Confidential	NA	NA
Shielded SSD	Confidential	NA	NA

Measurement Equipment & Software.

All data was collected with measurement equipment which has been calibrated by an ISO17025 accredited laboratory, where applicable, and was within the accredited usage period. A complete self-calibration was performed on each measurement device before connection to the DUT, and again upon completion of measurements utilizing a given DUT. This ensured that no measurement variance was due to a non-standard measurement device. Leading particulars for all measurement devices can be found in Table 3.

Table 3. Description of Signal Source and Measurement Equipment

Nomenclature	Manufacturer	Model Number
Near Field Scanner	Aprel	EM-ISight
Preamplifier	Aprel	APL-EMIS-AMP
Cable 1	Aprel	APL-CB3-20G
Cable 2	Aprel	APL-CB3-20G
Hz Field Probe, 6 GHz	Aprel	ALS-EMIS-P-H-M2.2
Ez Field Probe, 6 GHz	Aprel	ALS-EMIS-P-E-M2.2
Hz Field Probe, 20 GHz	Aprel	ALS-EMIS-P-H20G-M2.2
Signal Generator	Keysight	N5181B
Spectrum Analyzer	Keysight	N9020A
Signal Generator	National Instruments	PXIe-5654
PXIe Chassis	National Instruments	PXIe-1085
PXIe Controller	National Instruments	PXIe-8840
Comb Generator	York EMC	CGE02C
Battery Pack	York EMC	BP01

The table describes the leading particulars of the devices used to generate reference signals and to measure signals of interest.

Several pieces of software were used in the excitation of the Devices Under Test, for the measurement of the output of the devices under excitation, and in the post-processing of the data to simplify analysis. Leading particulars of the software and details of their implementation are found in Table 4.

Table 4. Description of Software for Excitation and Measurement

Nomenclature	Manufacturer	Version
EM-ISight	Aprel	4.5
Far-Field Approximation Toolset	Aprel	4.5
Radio Frequency Interference Toolset	Aprel	4.5
EMC Exerciser	SSD Manufacturer	NA

EMC Exerciser is an application developed by the SSD manufacturer for the purpose of putting the SSD in a state typical of the normal worst-case usage case that such a device would experience. It was configured with default settings and run during all SSD measurements

Far Field Approximation Toolset is provided by the manufacturer of the EM-ISight tool. Near-field measurements are taken in the Fresnel region, near a reference dipole surface, and extrapolated to mathematical results obtained using numerical methods. Performing these measurement in near field, as opposed to far field, permits accurate measurements without interference from external noise and other ambient interactions [8].

Radio Frequency Interference Toolset is provided by the manufacturer of the EM-ISight tool. It provides a method of assessing the result of complex E field and H field waves on a circuit design. This method was chosen as it allows the final analysis to be shown without time-dependencies of any stochastic signals present in the noise. The ability to collect data in a real-time environment allows identification of the field distributions across specific areas [9]

Additional Materials.

In the course of measurements, it was discovered that a material suitable for the absorption of radio frequency energy was desirable to limit the presence of electromagnetic waves which interfered with the measurement. Multiple samples were analyzed using the RF Absorption Effectiveness procedure. The material chosen was AB7730, made by 3M. Information from the product data sheet is shown in Figure X.

Methodology.

Measurements were designed to capture data which can drive conclusions through analysis. All measurements were accomplished in a 3 meter by 2 meter copper screen room, which was verified to have at least 100 dB of ambient shielding effectiveness according to MIL-STD 285. A description of the purpose of each measurement and the measurement configuration is given below.

Baseline Investigation.

The first measurement to accomplish was an investigatory measurement to understand basic properties of the material under excitation and to determine which of all possible successive measurements would provide the most meaningful data. Previous experiments to characterize the S21 of the material as a magnetic core on nano-scale inductors had been accomplished using a reference frequency of 2 GHz. In order to limit source-signal variance and provide verification of the frequency response characteristics previously documented, a signal generator was set to output a nominal 0 dBm, as measured after cable and connector loss at the input to the spectrum analyzer. This reference signal was launched from the injection point of the 6 GHz Magnetic Strip line. A measurement area of 10 mm X 10 mm was defined for sampling signals with 1mm of spacial resolution at a measurement height of 1mm. Each sample of at least 10 mm in each axis was then placed on the center of the measurement area, with the deposition side down, and the measurement was repeated. Placing the deposition side of the sample ‘face-down’ allows the gap between the strapline and the shielding to remain constant so

that the only variability induced by differing substrates is in the dielectric constant of the gap between the CoZrTaB layer and the measurement probe. The measurement configuration utilized for this measurement is shown below in Figure 3.

Figure 3. Baseline Measurement Setup

Lowered Power Baseline Investigation.

Analysis indicated that a signal at a 0 dBm level was radiating around the edges of each of the smaller samples and contributing to the levels measured over the sample. In order to correct for this observation and sample only the signal coupling through the material and substrate, the baseline measurement was repeated at signal level of -20 dBm, normalized to the launching point of the MSL. This level was sufficient to sample shielding effectiveness without polluting the measurement environment with unnecessary power.

Substrate Variance Investigation.

Due to the limitations of available samples, it was necessary to determine the variability of the shielding effectiveness induced in the measurement by the differing types of substrate, polyimide (Pi) and silicon (Si). There was only one deposition technique which was shared

across both substrates, five layers of 5 nanometers each (25 nm total CoZrTaB thickness). However, these samples had less than half of the available surface area of the smallest of the other samples. Therefore, a special measurement was designed to utilize these samples and control for all variability not associated with the substrate material. Each sample was placed deposition-side down at the center of measurement area defined in the Baseline Investigation and secured at diagonal corners with a small piece of polyimide tape. A sample of AB7730 RF absorption material was then fabricated to cover the area around the measurement sample, with an area removed from the middle of the absorption material to allow data sampling. This 'window' in absorption material provided sufficient noise dampening for the two smallest samples, and the technique was adopted for successive measurement of the larger samples using a larger piece of absorption material fabricated to the same basic shape.

The signal source for this measurement was the CGE01 Comb Generator. The output of this device is a band discrete signals spaced every 250 MHz from 1 GHz to 40 GHz. It was connected to the launching point of the 6 GHz MSL without consideration for cable loss, as this was to be a relative measurement and the problem of excessive power was not an issue, due to the lower power of the Comb Generator and the presence of the RF absorption material. The spectrum analyzer was configured to exclusively examine the continuous wave at 3.5 GHz. This frequency was chosen as the reference signal because this band is the presumptive home of the first generation of 5G devices, in both Stand-Alone (SA) and Non-Stand-Alone (NSA) variants of 5G radios. The resolution bandwidth and span were decreased to the smallest sampling window possible, which allowed analysis of the fundamental frequency, its upper and lower sidebands, and the intermodulation harmonics surrounding it. This allowed for analysis of a comprehensive modulated signal, similar wave shape and structure to a narrowband signal modulated for communication. Each sample was placed over the strapline, and a raster pattern of 1mm spacial resolution was accomplished at a 1.5 mm measurement height, with the probe rotated by 15

degrees in repeated passes. The data was collected and processed for analysis by the EM-ISight software, and the measurement was then repeated for the other sample.

Broadband Discrete Noise Investigation, 1 GHz – 6 GHz.

In order to understand the shielding effectiveness performance of the material under test in the most common communication and regulatory measurement bands. All regulatory agencies for any country in the world require measurements for unintentional radiation in the band from 1 GHz – 6 GHz. This band is also the most populated civilian communication band. Cellular, Wi-Fi, cordless phones, satellite TV and radio, Bluetooth, LoRA, ZigBee, etc. utilize this band, in addition to communication systems used by Police and other First Responders.
The signal source for this measurement was the CGE01 Comb Generator. The output of this device is a band discrete signals spaced every 250 MHz from 1 GHz to 40 GHz. It was connected to the launching point of the 6 GHz MSL without consideration for cable loss, as this was to be a relative measurement and the problem of excessive power was not an issue, due to the lower power of the Comb Generator and the presence of the RF absorption material. Each sample was placed over the strapline, and a raster pattern of 1mm spacial resolution was accomplished at a 1.5 mm measurement height, with the probe rotated by 15 degrees in repeated passes. Each sample was measured in turn. The spectrum analyzer was configured to exclusively examine the band from 1 GHz to 6 GHz. The spectrum analyzer's average detector was used for sampling the signal, to minimize the contribution of spurious or non-determistic noise. The Root-Mean Square of 10 samples was recorded by the analyzer and collected by EM-ISight software. Each measurement peak was manually selected, and data was output for analysis. Measurement configuration is shown in Figure 4.

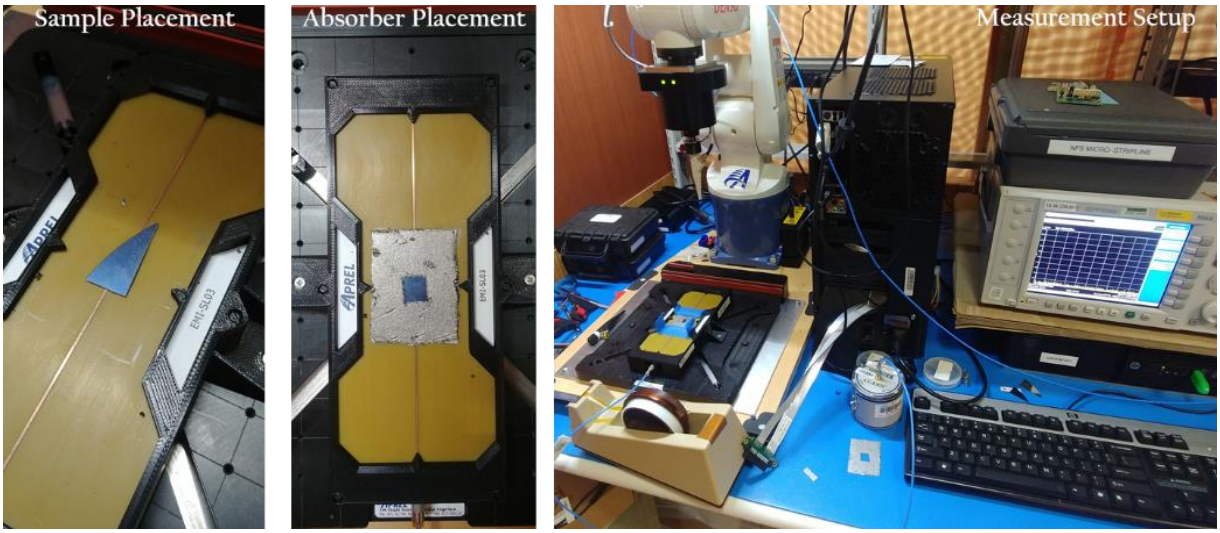

Figure 4. Measurement Configuration, Broadband Discrete Noise, 1-6 GHz

Broadband Discrete Noise Investigation, 20 GHz - 24 GHz.

In order to understand the shielding effectiveness performance of the material under test in a band licensed for 5G communication systems, effort was made to characterize the material in the 20 GHz – 24 GHz band. This mm-wave band will be highly populated with ultra-broadband (>1 Gbs mobile, > 10 Gbs stationary) devices used for streaming 4k or other UHD video, augmented or virtual reality, in-vehicle infotainment, and other 'big data' applications.

The signal source for this measurement was the National Instruments Signal Generator, housed in a PXIe chassis, controlled by a National Instruments Quad-Core. The output of this device is a discrete signal 20 GHz. It was connected to the launching point of the 20 GHz MSL without consideration for cable loss, as this was to be a relative measurement and the problem of excessive power was not an issue, due to the maximum output power of the device. Each sample was placed over the strapline, and a raster pattern of 1mm spacial resolution was accomplished at a 1.5 mm measurement height, with the probe rotated to 0 degrees and 90 degrees for measurement. Each sample was measured in turn. The spectrum analyzer was configured to

exclusively examine the signal at 20 GHz. The spectrum analyzer's average detector was used for sampling the signal, to minimize the contribution of spurious or non-determistic noise. The Root-Mean Square of 10 samples was recorded by the analyzer and collected by EM-ISight software. Each measurement peak was manually selected, and data was output for analysis.

In-Situ Worst-Case Typical Noise Investigation.

In order to understand the performance of the material in an environment of complex and overlapping waves, a test was designed to investigate the shielding effectiveness and field effects on an actual device. One of the challenges of this experiment was finding a suitable DUT, we would need a device representative of one which could be found in the near-future 5G, which would also fit in our available measurement volume and have documented worst-case typical use cases. Ideally, it would be typically shielded as deployed in the market, but have an unshielded available for shielding with CoZrTaB for direct comparison. The DUT selected is an SSD from a leading manufacturer, and it meets all of the criteria, including shielded and unshielded samples. However, as a pre-production device, the quantification of the data has been redacted as it is not for publication.

The DUT was placed on a purpose-built PCIe-extender and connected to a host computer via a PCIe extender cable. The EMC Exerciser was configured to sequentially write, read, then erase a 100 Mb file. The spectrum analyzer was configured to exclusively at the selected signal, and the drive activity was monitored. A preliminary broadband scan of the H-Field was collected for all frequencies below 6 GHz at a measurement height of 1 mm and 45 degrees of probe theta resolution. The frequency of 1150 MHz was selected for analysis. A raster pattern of 1 mm spacial resolution was accomplished at a 1.5 mm measurement height with, with the probe rotated by 15 degrees in repeated passes. Successive passes at increasing heights were accomplished in order to approximate the far field effect of the material on a device using the Far-Field Approximation (FFA) software. The H-field probe was then replaced with the E-Field

probe and the measurement repeated in order to collect sufficient information to perform a Radio Frequency Interference analysis. A piece was cut from the large sample of the 10 X 50 nm Pi to the size of the DUT, and was placed over the SSD. Measurements for FFA and RFI analysis were repeated for the DUT as shielded by the sample. Figure

Figure 5. Measurement Configuration, In-Situ Worst-Case Typical Noise

Chapter 3 RESULTS AND DISCUSSION

As expected, the difference in substrate exhibited almost no relative effect on the fields of interest or their measurement. The material exhibits exemplary shielding effectiveness in all tests where results were attainable. Detailed results and discussion of each test follows.

Baseline Investigation.

Baseline investigation revealed that the injected signal was too high for the size of the samples, leading to power radiating around the sample and interfering with the measurement of the energy passing through the material. Power was lowered to a reference signal of -20 dBm and the issue was resolved.

Lowered Power Baseline Investigation.

The samples exhibited excellent shielding effectiveness, and also appeared to re-orient the lines of flux in the magnetic field to orthogonal to the direction of sputter deposition. The largest sample size exhibited the most dramatic attenuation of the propagating wave, but that is more easily explained by the mitigation of waves in a larger area around the measured area than it is to the unique shielding abilities of the 10 X 50 nm sputtering technique, as this result was not realized by 2 GHz measurement in the Broadband Discrete Noise Investigation.

Substrate Variance Investigation.

The substrate had little discernable impact on the amplitude or shape of the waveform under investigation. There does appear to be a slight increase in the noise amplitude in the silicon substrate, which coincides with a marginal decrease in the amplitude of the peak. This is slight variance is likely due to the fact that the silicon substrate is ten times thicker than the polyimide. Test results for magnetic films deposited on Polyimide substrate and Silicon substrate are shown in Figure 6 and Figure 7, respectively.

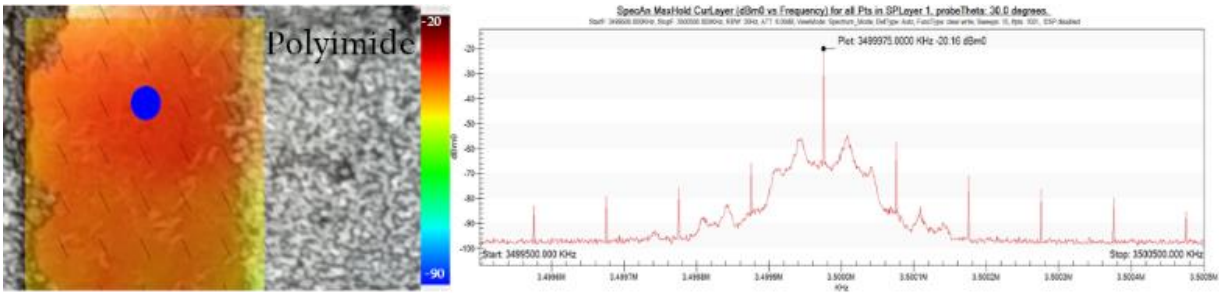

Figure 6. Polyimide Substrate Performance

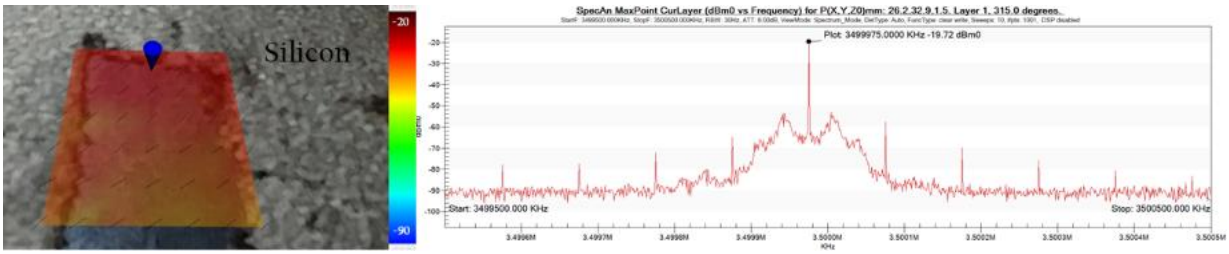

Figure 7. Silicon Substrate Performance

Broadband Discrete Noise Investigation, 1 GHz – 6 GHz.

Results for this investigation are shown in Figure 7.

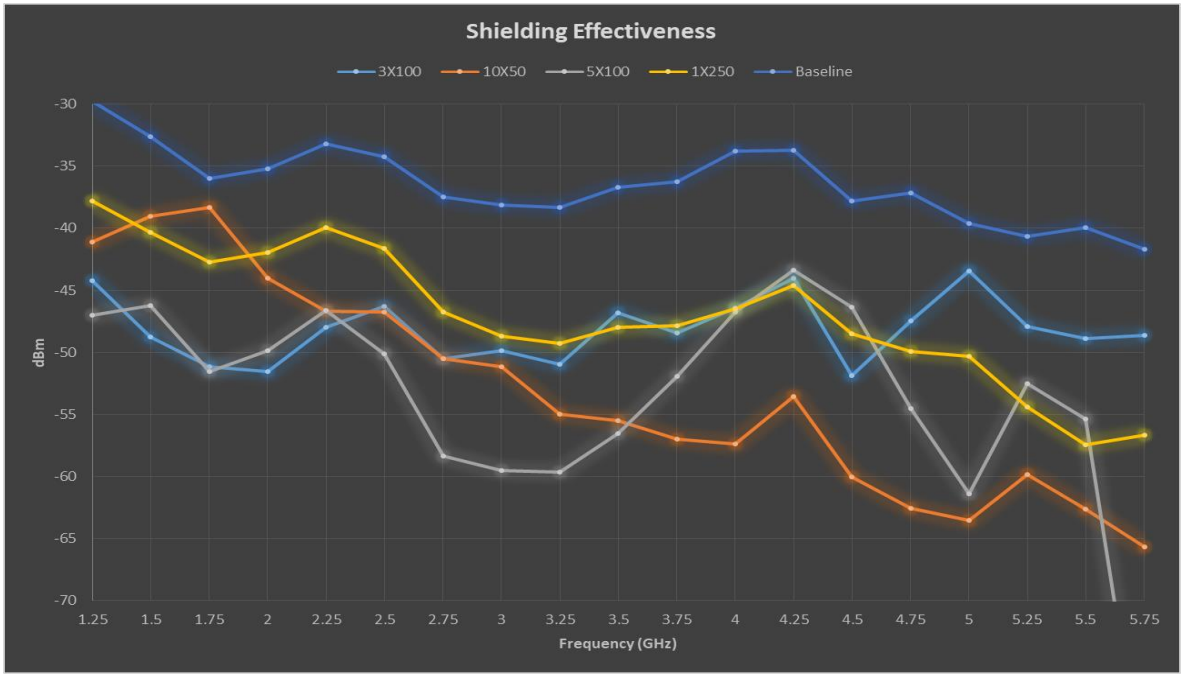

Figure 8. Shielding Effectiveness by Sample

All measurements were taken at a measurement height of 1.5 mm above the magnetic strip line, using the Hz probe. The first point of note is the excellent shielding effectiveness of the material at all frequencies. All samples are at least 3 dB below the baseline measurement at all frequencies. Average shielding effectiveness across all samples and frequencies was an average of 13.9 dBm. This average obvious outlier for the material sample of 3 X 100 nm layers at a frequency of 1.575 GHz. This data point is probably due to an imperfection in the sputtering or possibly due to mechanical defect induced by the repeated handling involved in this and prior experiments. Figure 8 shows the location of the null value in the middle of the sample, but values around the null are in between the values of the 1 X 250 nm (250 nm total) and the 10 X 50 nm (500 nm total) samples.

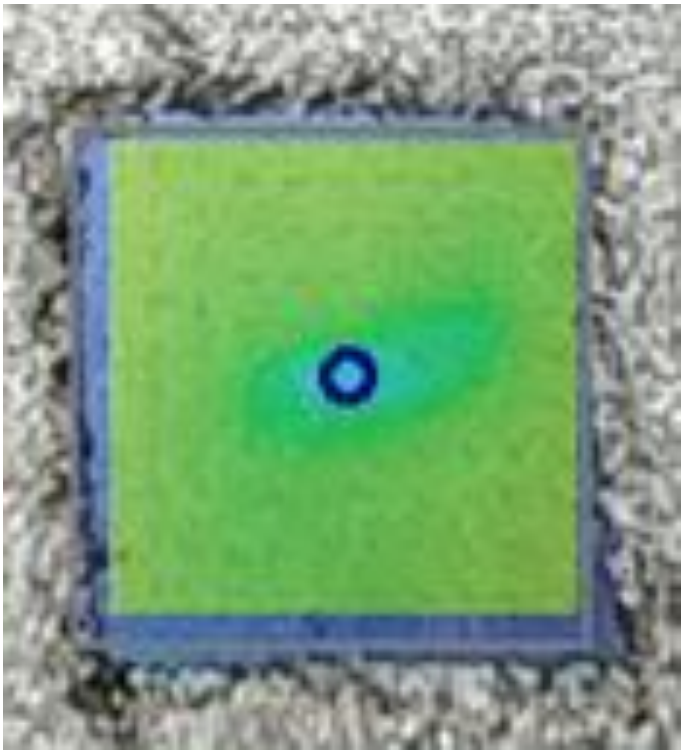

Figure 9. Location of Outlier Value in 3 X 100 nm Sample

However, the lines of flux appear to be circular around the null location, a behavior not observed in the 2 GHz scan. More samples will be required to identify if this is a feature of the material or a defect of the sample.

Broadband Discrete Noise Investigation, 20 GHz - 24 GHz.

Due to the small size of the MSL and the relatively large size of the samples, shielding effectiveness and other field characterization measurements were not successful. The close proximity of the reference plane paths on either side of the strapline meant that any conductor placed over the strapline provided a return path to ground. As such, any metal placed over the strapline would cause an increase in the amplitude at the measurement device, as the signal being measured was the return signal, and it was much closer to the probe. Future experiments will identify a different radiating mechanism to replace the MSL in this measurement, or will require a sample specifically designed to overcome the limitations of this radiation source.

In-Situ Worst-Case Typical Noise Investigation.

The unshielded reference signal exhibited typical behavior of a complex electromagnetic field excited by a high-speed digital data bus, and is shown in Figure 9.

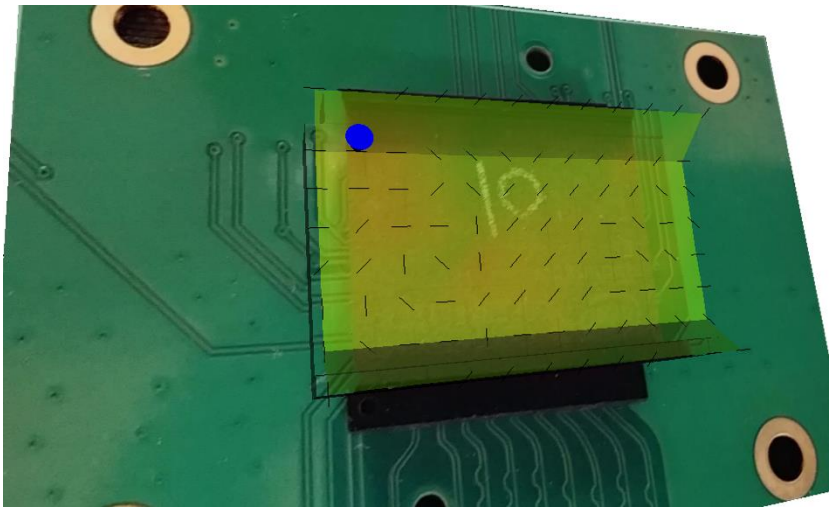

Figure 10. Unshielded SSD Reference, H-Field

The shielded sample exhibited effective shielding, and did not have a significant impact on the direction of the lines of flux in the standing waves in near-field. The shielded example consists of a typical sputter-deposited metal film, significantly thicker than the 500 nm of total CoZrTaB deposited on the sample for comparison. The shielded example also has the benefit of being fully bonded to all 5 available surfaces by the sputter deposition process. The CoZrTaB sample was simply cut to fit the area available on the top of the SSD and between the sides of the mounting mechanism. Shielding effectiveness for the shielded sample is shown in Figure 10.

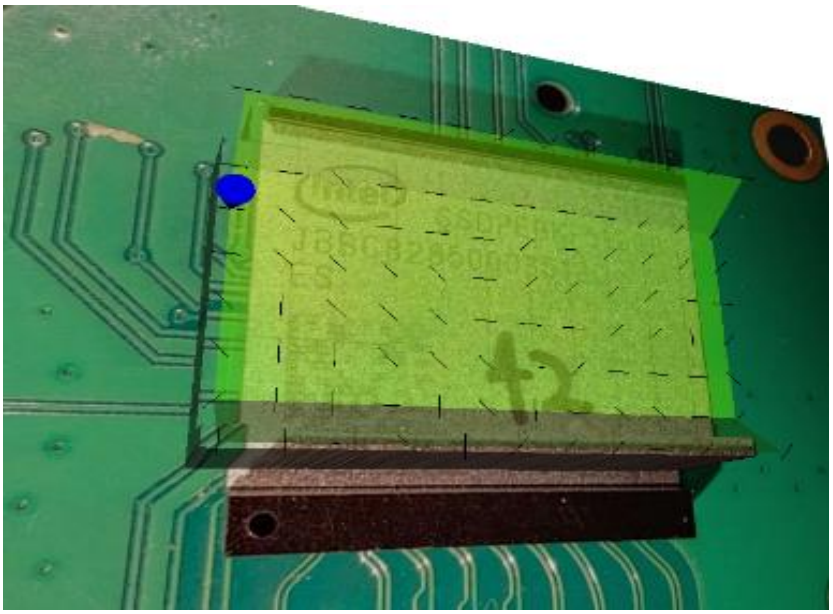

Figure 11. Shielded SSD Reference, H-Field

Analysis of the vector distribution of the fields was accomplished using the RFI Approximation test methodology, measurements were taken at Z-heights of 1.5 mm for Layer 1 and at 6.5 mm for Layer 2. Characterization data was data for the device, and then a sample of 10 X 50 nm (500 nm total thickness of CZTB) was cut to fit the exact size of the top layer of the SSD, and was placed on the device. Using the exact measurement setup as the unshielded reference, all E-field and H-field measurements were accomplished again. Figure 11 shows the unshielded reference, and Figure 12 shows the shielded experiment. The figures show the direction and magnitude of the highest E field or H field strength for a given measurement coordinate. The presence of what are apparently two sources for the 1150 MHz was apparent from the analysis of Figure 11, as there are two distinct wave structures. One wave structure originates between the 25 and 30 mm height, and the other just below the 25 mm demarcation. This is further realized by the wide dispersion of vector angles, especially notable in the upper left corner of Figure 11. Comparison to the vectors in Figure 12 shows a much more consistent vector orientation, especially as the energy is sampled further away from the source in the upper

left corner. Additionally, the material appears to have limited the interaction of the fields, as evidence by the lack of a common orange area between the two sources. This area is present in the coordinate area of (23, 25) on Figure 11, and vector magnitude indicates that the fields are joining in the unshielded sample. However, that same area of the shielded sample shows that not only has the orange overlap area been replaced by a thin aqua line between the sources at the same coordinate location in Figure 12, but that the vector lines are oriented in completely opposite directions.

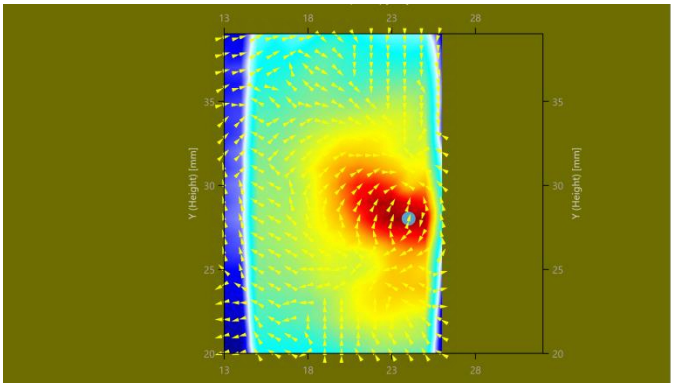

Figure 12. Unshielded H field vector distribution, Layer 1

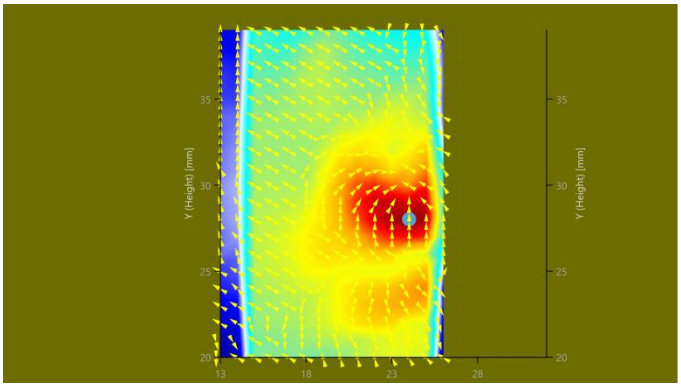

Figure 13. Shielded H field vector distribution, Layer 1

Much of the same behavior can be seen in Layer 2 for the H field measurement. Figure 13 shows the unshielded reference, and Figure 14 shows the shielded experiment. The vector

distribution and orientation is varied across the surface of the unshielded device, especially around the location of the peak amplitude. Although the peak recorded in the shielded sample was .7 dB higher, all of the field vectors have been oriented 0 degrees, and the energy is more dispersed across the layer.

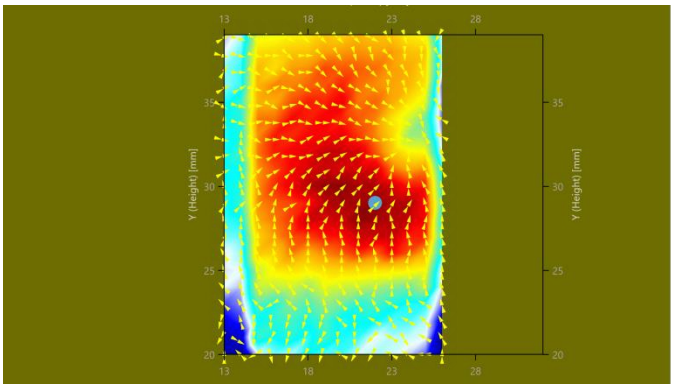

Figure 14. Unshielded H field vector distribution, Layer 2

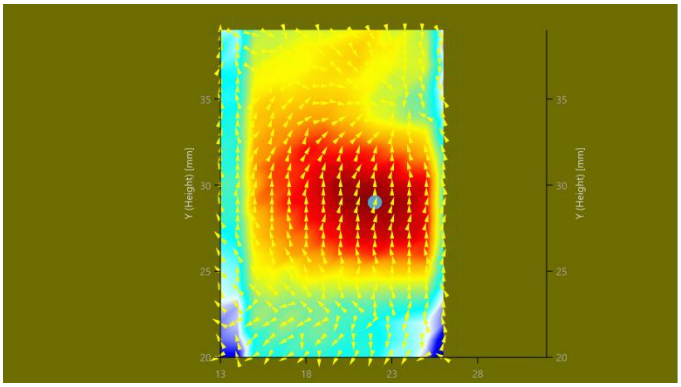

Figure 15. Shielded H field vector distribution, Layer 2

For analysis of Layer 1 of the E field, Figure 15 shows the unshielded reference and Figure 16 shows the shielded experiment. The first point of note is that the field distribution is much more uniform across the surface, even though the peak recorded value is a marginal .7 dB higher. This indicates that the material under experiment is accumulating a minor charge, but this stored charge is realized as a new distribution, direction, and orientation of the field vectors.

Also apparent in these figures is the close proximity of two sources in the lower right corner of the figures. As in the H field analysis, the interaction of the two sources is simplified and mostly segregated by the presence of the film.

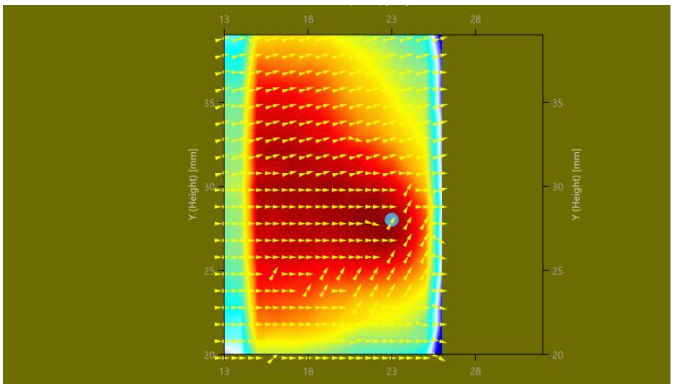

Figure 16. Unshielded E field vector distribution, Layer 1

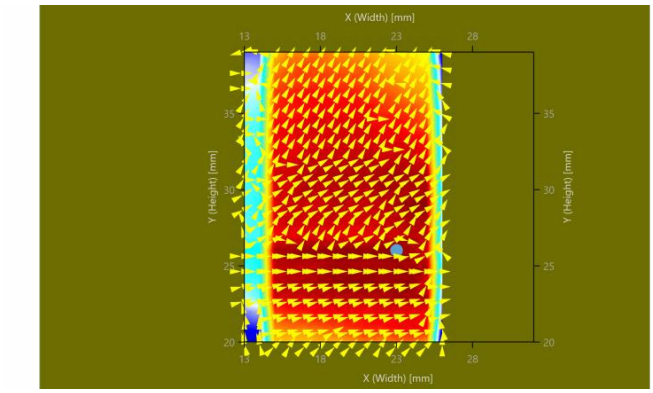

Figure 17. Shielded E field vector distribution, Layer 1

When analyzing Layer 2, the same behavior of the material is noted. In the unshielded reference shown in Figure 17, the peak is slightly lower (.4 dB) than the peak recorded with the material sample covering the SSD. Despite the increase in the peak, the field is more evenly dispersed throughout the layer as shown by nearly equal distribution of magnitudes.

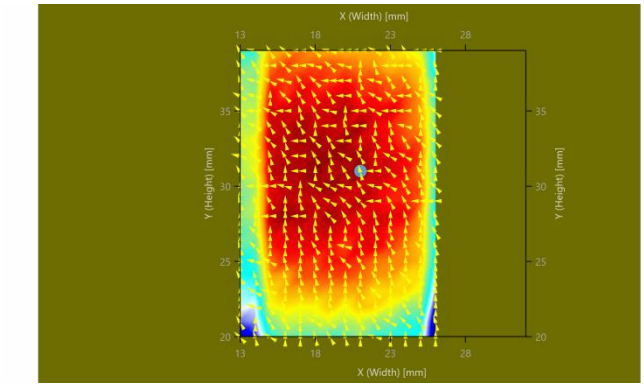

Figure 18. Unshielded E field vector distribution, Layer 1

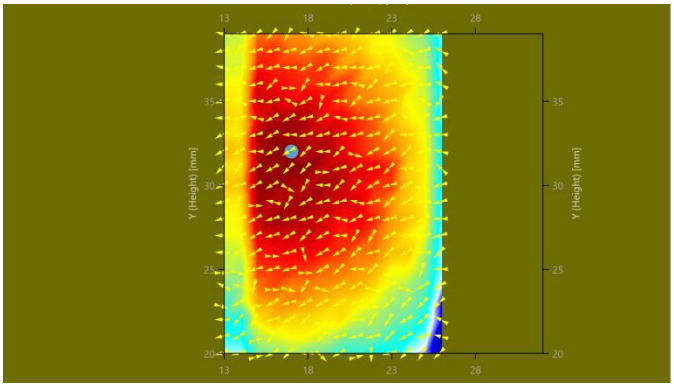

Figure 19. Unshielded E field vector distribution, Layer 1

To understand the aggregated directivity of the above figures, we utilize a directivity diagram. The directivity diagram shows the maximum vector in each direction from all scans on the measurement layer, which yields the directivity of the signal over a polar plot. Figure 19 shows the directivity of the E field and the H field for the unshielded reference, and Figure 20 shows the directivity of the SSD when shielded with CZTB. The E field is shown in Green and the H field is shown in Red. The first and most obvious delta is the change in the shape and orientation of the E field's directivity. This indicates a change in the distribution of energy between the two noise sources. The green circle of the E field is also more circular in the

shielded sample, indicating a more uniform distribution of energy. Also, the null present in both directivity diagrams has rotated by 90 degrees, being oriented in the direction of 90 degrees in the unshielded sample, but oriented to 180 degrees in the shielded sample. While the magnitude of the vectors clearly indicates that this is a predominantly H field signal, the directivity of the red circle showing H field is also more uniformly distributed around the plot, and the peak has rotated by approximately 15 degrees. The shape of the shielded directivity plot has more magnitude in the top half of the plot, while the unshielded sample shows peaks at the 350 degree and 160 degree orientations.

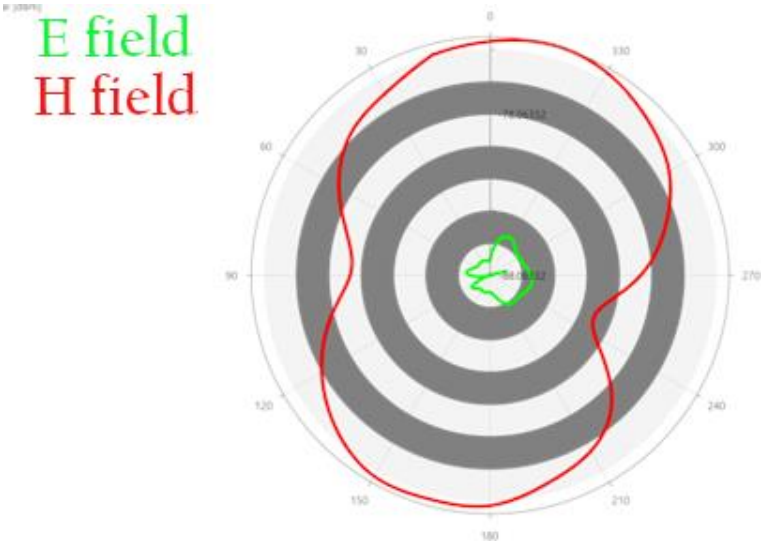

Figure 20. Unshielded Directivity Diagram, Layer 1

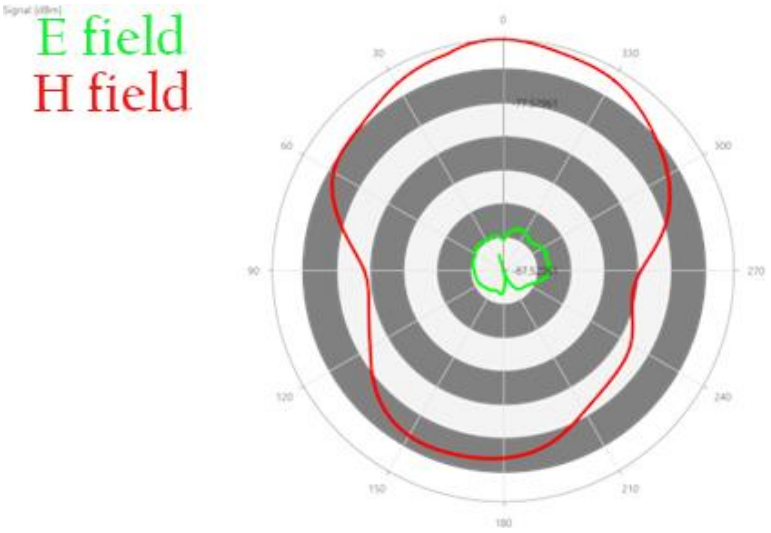

Figure 21. Shielded Directivity Diagram, Layer 1

In the Layer 2, there is no such domination by one field. Yet the results are even more dramatic. In the unshielded reference shown in Figure 21, the green E field is fairly circular and evenly directed. It could be characterized as being isotropic in all directions, and showing omni-directivity. In contrast, the red shape of the H-field is biased in the direction of 315 degrees, with a distinct lack of energy in the 120 degree orientation. When compared to the shielded example shown in Figure 22, the variation is significant. The green E field has been completely oriented to the direction of 0 degrees – 90 degrees. The red H field has been distributed nearly uniformly in all directions. If the E field and the H field are orthogonally related in the near field, they will propagate to the far field, and depending on the amplitude may extend far off of the radiating surface. The presence of the material is creating its own fields, with resultant eddy currents on the surface. These inducted currents create E fields that will constructively or destructively interfere with other E fields. The presence of the material changes the phase orientation of the field, and by changing the coupling orientation affect which waves will be resonant and which waves will be evanescent.

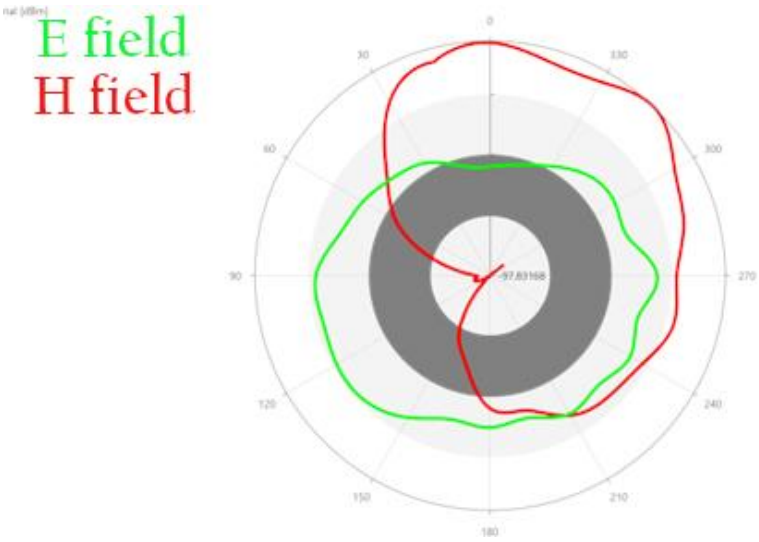

Figure 22. Unshielded Directivity Diagram, Layer 2

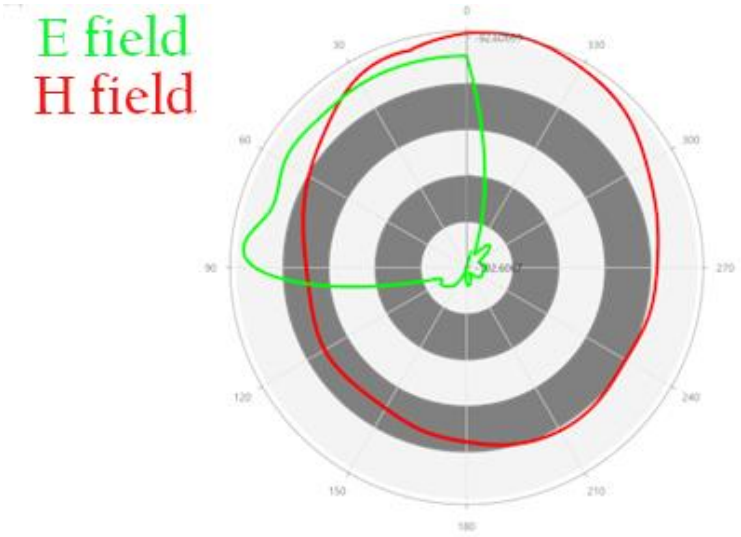

Figure 23. Unshielded Directivity Diagram, Layer 2

Analysis of the wave propagation properties were calculated using FFA and RFI software tools. Results for the unshielded reference are shown in Figure 23, and the results for the shielded experiment are shown in Figure 24. Unfortunately, the frequency selected for analysis, 1150 MHz, did not propagate in to the far field. Lacking a resonant mode, it remained an evanescent field on the surface of the device with insufficient energy to radiate through free space. The relatively long time for RFI measurement, coupled with the inconsistent stability of

the test setup, meant that examining and selecting other frequencies for FFA and RFI analysis was not a feasible option. In the unshielded reference, the two sources stayed closely co-located and their energy remained focused at the source. When the shielding material was applied to the top of the SSD, the material accumulated energy and redistributed charge. This is evidenced by the dispersion of the sources in to two concentric circles, a high energy red area and a lower energy yellow area. Additionally, the entire surface of the shielded experiment contains energy, while the edges of the unshielded sample contain none. The result of this storage and redistribution of energy is shown in more detail by analysis of the backscatter of the signal.

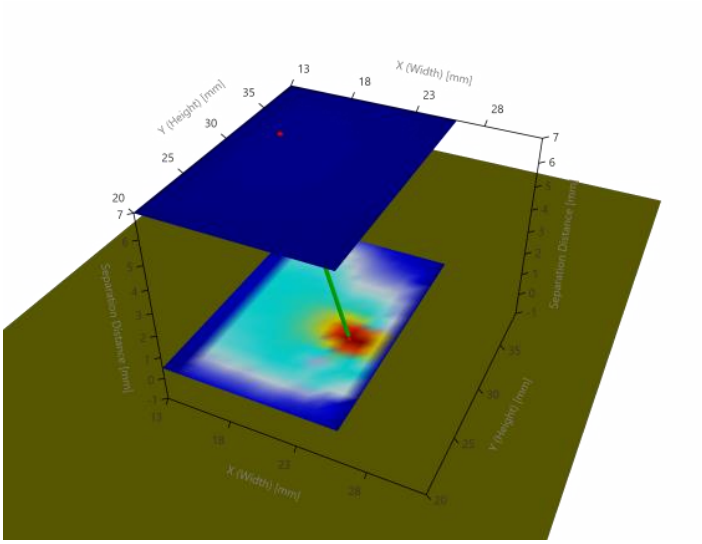

Figure 24. Unshielded Wave Propagation

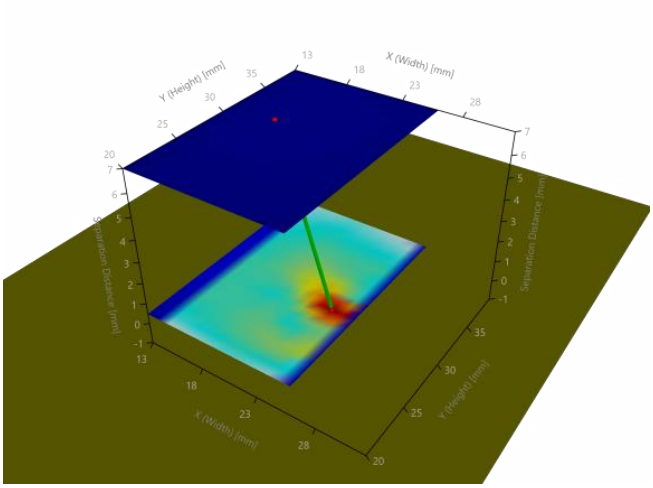

Figure 25. Shielded Wave Propagation.

The backscatter analysis is shown in Figure 25 and Figure 26 for the unshielded reference and the shielded experiment, respectively. A large portion of the energy is in the upper right corner of the sample, and the two sources are highly interactive. When shielding is applied over the surface, the two sources become segregated and the energy is more evenly distributed over the surface. At the upper measurement layer, the shielded example has nearly perfect uniformity in the distribution of energy. Additionally, this is accomplished without reflecting significant energy back in to the device, which is a common problem with traditional shielding. The results of this experiment indicate that only 6% of the energy is being distributed on the surface or backscattered.

CHAPTER 4 CONCLUSIONS AND RECOMMENDATIONS

The results of the experiments presented here clearly show the exceptional shielding effectiveness of the thin magnetic material. This study shows a 10 dB attenuation of fields in the presumptive 5G radio band, with less than half of a micron of material thickness, and without the benefit of encompassing the entire DUT with shielding. Additionally, the material showed the unique property of holding and redistributing charge along the orientation of sputter deposition. This property of the material, coupled with its very effective shielding in the 2 GHz – 3 GHz range, means that it may have application in shielding highly sensitive components, such as crystal oscillators, from the harmful effects of Electro-Static Discharge (ESD) events. Additionally, the charge distribution and shielding characteristics may find further application in eliminating the interference and cross-talk problems commonly associated with evanescent fields on high speed digital data buses.

The limitation on the conclusions of the study were the restrictions on experimental samples. With this new understanding of the of the near and far field effects of the CoZrTaB material on electromagnetic fields and waves, experiments can be designed to investigate specific unique properties and draw conclusions regarding the applicability of the material to a whole host of interference issues.

References

[1] Statistiscs Dictionary. (n.d.). Retrieved from https://stattrek.com/statistics/dictionary.aspx?definition=type%20ii%20error

[2] Brown, Gabriel, "5G & Industrial Automation: Creating the Factory of the Future" (2018). *LightReading*. Page 4. Retrieved from https://www.lightreading.com/iot/industrial-iot/5g-and-industrial-automation-creating-the-factory-of-the-future/a/d-id/743826

[3] Eadie, Andy, "RF Modules – Pre-certified vs. Non-Certified and How to Design Your Own" (2014). *EMC FastPass*. Page 30. Retrieved from https://emcfastpass.com/rf-modules/

[4] Morrison, R., Solving Interference Problems in Electronics, First Edition, John Wiley & Sons, 1996, Page 42.

[5] J. Choi, X. Cao, and D. Maslyk, "Component Level EMI Shielding for Semiconductor Packages," (2017). Henkel and Associates. Page 26. Retrieved from http://henkeladhesivesna.com/iframes/emi_shielding_solutions/documents/webinar-henkel-package-level-emi-shielding-external.pdf

[6] Brewer, Ron, "Designing an RF Shielded Enclosure" (2007). Interference Technology. Retrieved from https://interferencetechnology.com/designing-rf-shielded-enclosure/

[7] G. Fenical and P. Crotty, "Technology Advancements in Board Level Shields for EMI Mitigation: Not Your Daddy's Metal Can" (2012). InCompliance. Retrieved from https://incompliancemag.com/article/technology-advancements-in-board-level-shields-for-emi-mitigation-not-your-daddys-metal-can/

[8] D. Brooks, S. Nichol, J. Hones, and J. Lee, "Near-field Magnetic Probe Method Predicting Far-field Measurements — Correlation of Dipole Boresight Measurements with Anechoic Range Model" (2013). PIERS. Page 2-4.

[9] Nesterova, Marnya, "Experimental Assessment of Stochastic Signals Through the Power Density Method" (2018). EMC-SIPI. Page 1-3